HHS Public Access

Author manuscript

Acad Radiol. Author manuscript; available in PMC 2018 December 04.

Published in final edited form as:

Acad Radiol. 2017 July ; 24(7): 867–875. doi:10.1016/j.acra.2016.12.014.

Diagnosis of Spinal Lesions Using Heuristic and Pharmacokinetic Parameters Measured by Dynamic Contrast-Enhanced MRI

Ning Lang, MD, **Huishu Yuan, MD**, **Hon J. Yu, PhD**, and **Min-Ying Su, PhD**

Department of Radiology, Peking University Third Hospital, 49 North Garden Road, Haidian District, Beijing 100191, China (N.L., H.Y.); Tu & Yuen Center for Functional Onco-Imaging, Department of Radiological Sciences, University of California, Irvine Hall 164, Irvine, CA 92697-5020 (H.J.Y., M.-Y.S.)

Abstract

Rationale and Objectives: This study aimed to evaluate the diagnostic performance of dynamic contrast-enhanced magnetic resonance imaging (DCE-MRI) in differentiation of four spinal lesions by using heuristic and pharmacokinetic parameters analyzed from DCE signal intensity time course.

Materials and Methods: DCE-MRI of 62 subjects with confirmed myeloma (n=9), metastatic cancer (n= 22), lymphoma (n= 7), and inflammatory tuberculosis (TB) (n= 24) in the spine were analyzed retrospectively. The region of interest was placed on strongly enhanced tissues. The DCE time course was categorized as the “wash-out,” “plateau,” or “persistent enhancement” pattern. The maximum enhancement, steepest wash-in enhancement, and wash-out slope using the signal intensity at 67 seconds after contrast injection as reference were measured. The Tofts 2-compartmental pharmacokinetic model was applied to obtain K^{trans} and k_{ep}. Pearson correlation between heuristic and pharmacokinetic parameters was evaluated, and receiver operating characteristic curve analysis was performed for pairwise group differentiation.

Results: The mean wash-out slope was −22% ± 10% for myeloma, 1% ± 0.4% for metastatic cancer, 3% ± 3% for lymphoma, and 7% ± 10% for TB, and it could significantly distinguish myeloma from metastasis (area under the curve [AUC] = 0.884), lymphoma (AUC = 1.0), and TB (AUC = 1.0) with P = .001, and distinguish metastasis from TB (AUC = 0.741) with P = .005. The k_{ep} and wash-out slope were highly correlated (r = 0.92), and they showed a similar diagnostic performance. The K^{trans} was significantly correlated with the maximum enhancement (r = 0.71) and the steepest wash-in enhancement (r = 0.85), but they had inferior diagnostic performance compared to the wash-out slope.

Conclusions: DCE-MRI may provide additional diagnostic information, and a simple wash-out slope had the best diagnostic performance. The heuristic and pharmacokinetic parameters were highly correlated.

Address correspondence to: H.Y. huishuy@bjmu.edu.cn; M.-Y.S. msu@uci.edu.

Keywords

Dynamic contrast-enhanced MRI; DCE kinetic pattern; pharmacokinetic analysis; spinal lesion diagnosis; wash-out slope

INTRODUCTION

Dynamic contrast-enhanced magnetic resonance imaging (DCE-MRI) is the standard method widely used for diagnosis of breast and prostate cancer (1,2). Because it can be easily performed, many studies have applied this method to characterize soft tissue lesions in other organs (3,4). In this study DCE-MRI was used to characterize four lesions in the spine, including myeloma, metastatic cancer, lymphoma, and inflammatory tuberculosis (TB). In DCE-MRI, multiple sets of images were acquired before and after injection of contrast agents, and the measured signal intensity time course (or, the enhancement kinetics) reflected the vascular and cellular properties of the lesion. The heuristic parameters, such as maximum enhancement, wash-in slope, and washout slope can be directly measured from the DCE kinetics. The more sophisticated two-compartmental model can be used to analyze the transport of contrast agents between the vascular space and the interstitial space to obtain pharmacokinetic parameters such as K^{trans} and k_{ep} (5,6). Many different methods have been applied to analyze the DCE kinetics, but there is no consensus on which method is the best (4,7). It is in general agreed that as long as characteristic parameters can be reliably extracted, they may provide helpful information for a correct diagnosis as well as surgical planning.

DCE-MRI has been applied to diagnose different spinal lesions (8–11) and distinguish between hypervascular (eg, renal cell carcinoma) and hypovascular (eg, prostate cancer) metastases (12,13). It has also been used to characterize vascular properties of hematologic malignancies (eg, myeloma and lymphoma) with different grades of bone marrow involvement, as well as to evaluate changes after various therapies for predicting treatment outcome and prognosis (8,9,14–20). These studies used different DCE-MRI analysis methods to generate heuristic parameters or pharmacokinetic parameters. So far there is no published study to systematically compare the different DCE parameters for spinal lesions analyzed using different approaches. The purpose of this study is to investigate the correlation of DCE-MRI parameters obtained by using heuristic and pharmacokinetic analyses and to investigate further their diagnostic performance for differentiating four spinal lesions. The obtained DCE-MRI diagnostic parameters may provide information for characterizing the extent of disease for guiding biopsy and planning of surgery and subsequent adjuvant treatments.

MATERIALS AND METHODS

Patients

A total of 62 patients were analyzed in this study, including 9 patients with myeloma (58 ± 3 years old, [mean ± standard deveation]), 22 patients with metastatic cancer (55 ± 13 years old), 7 patients with spinal lymphoma (46 ± 19 years old), and 24 patientswithTB(43

± 18yearsold).Themetastaticcancersincluded seven lung, five thyroid, four liver, three breast, two kidney, and one prostate. All myeloma, metastatic cancer, lymphoma, and 21 of 24 TB were histologically proven. Three of 24 TB were confirmed by the good response to TB medication. Almost all patients had some pain symptoms, and on MRI, the most commonly observed features were vertebral bone destruction and soft tissue masses compressing the spinal cord. This study was approved by our Medical Ethics Committee. For this retrospective study, the informed consent was waived.

MRI Protocol

MRI scans were performed on a 3T scanner (Trio, Siemens, Erlangen, Germany). After the abnormal region was identified on precontrast images, DCE-MRI was performed using the three-dimensional volume interpolated breath-hold examination sequence in the transversal plane to further examine that region. The imaging parameters were repetition time (TR) = 4.1 milliseconds, echo time (TE) = 1.5 milliseconds, flip angle = 10°, acquisition matrix = 256 × 192, and field of view (FOV) = 250 × 250 mm. Approximately 30 slices with 3-mm thickness were prescribed to cover the abnormal vertebrae. The temporal resolution varied from 10 to 14 seconds. The contrast agent, 0.1 [mmol/kg] Gd-DTPA, was injected after one set of precontrast images was acquired, by using an Ulrich power injector at a rate of 2 mL/s followed by 20-cc saline flush at the same rate. A total of 12 frames were acquired, so the total DCE-MRI acquisition time period ranged from 120 to 168 seconds. Depending on the abnormal area that needed to be covered and the choice of sequences to acquire different views, the total imaging time was approximately 25–30 minutes.

Heuristic Parameters Analyzed From DCE Kinetics

For each case, the signal intensity time course was measured using the MeanCurve function on the Siemens scanner console using syngo MR B17 version software (Erlangen, Germany). One radiologist evaluated the contrast-enhanced images of the lesion on the axial view. Depending on the size of the lesion, strong enhancements could be seen on multiple DCE-MRI slices. The radiologist would evaluate the intensity of enhancements and decide one slice that showed the strongest enhancement and manually drew the region of interest (ROI). For cases that showed strong comparable enhancements on multiple slices, the radiologist would draw ROIs on different slices and chose one that showed the strongest enhancement with less noise (ie, smooth signal intensity time curve) for the analysis. For patients who had multiple lesions in different spine segments seen on the sagittal view, only the most clinically significant lesion (ie, the largest and that showed strong abnormal signal intensity) was chosen for the DCE-MRI study, and the analysis was done only for this lesion. The ROI size was from 0.5 to 1 cm^2, and caution was taken to exclude cysts, calcification, necrosis, and hemorrhage.

The signal intensity time course was evaluated to find the precontrast signal intensity (S_0), the maximum intensity (S_{max}), and two adjacent wash-in time points that showed the largest difference in their intensities (S_2 and S_1). Two heuristic DCE parameters were calculated as follows:

$$\text{Maximum Enhancement Ratio} = \left[\left(S_{max} - S_0\right)/S_0\right]$$

$$\text{Steepest Wash-in Enhancement Ratio} = \left[\left(S_2 - S_1\right)/S_0\right]$$

For cases with clearly visible peak enhancement that occurred around 67 seconds after injection (a time point in the DCE time course), the wash-out slope was calculated using the peak (S_{peak}) and the signal intensity at the last time point (S_{last}). For cases that did not show a peak before 67 seconds, the slope between the signal intensities at the 67 seconds time point ($S_{67seconds}$) and the last time point was calculated. Therefore, the wash-out slope percentage is calculated as follows:

$$\text{Wash-out Slope} = \left[\left(S_{last} - S_{peak}\right)/S_{peak}\right] \times 100\% \text{ or, } \left[\left(S_{last} - S_{67seconds}\right)/S_{67seconds}\right] \times 100\%$$

Based on the wash-out slope calculated by this definition, the DCE pattern was determined as “wash-out” when the slope showed >10% decrease, “persistent enhancement” when the slope showed >10% increase, and “plateau” when the change was smaller than 10%. Figure 1 shows four case examples, a myeloma showing the wash-out pattern, a metastatic cancer showing the plateau pattern, a lymphoma showing the plateau pattern, and a TB showing the persistent enhancement pattern.

Pharmacokinetic Analysis to Obtain K^{trans} and k_{ep}

The Tofts two-compartmental pharmacokinetic model was applied to obtain K^{trans} and k_{ep} (5,6) by using the populationaveraged fast, medium, and slow blood curves as references (21–23). In general, it is agreed that when the patient does not have diseases that would substantially alter the renal and cardiac function, or the hemodynamic circulation, using the population-based blood curves as references is a reasonable approach (24,25). The concentration of the [Gd] contrast agents in the blood was assumed to follow a bi-exponential decay function:

$$C_b = D\left[a_1 \exp\left(-m_1 t\right) + a_2 \exp\left(-m_2 t\right)\right]$$

where D was the injection dose, 0.1 [mmol/kg]. The parameters used for fast, medium, and slow blood curves were taken from the commercial DCE analysis program SygnoTissue4D (Siemens Healthcare, Erlangen, Germany). For the fast blood curve, a_1 = 92.0 [kg/L], a_2 = 6.4 [kg/L], m_1 = 5.3 [1/min], and m_2 = 0.016 [1/min]; for the medium blood curve, a_1 = 24.0 [kg/L], a_2 = 6.2 [kg/L], m_1 = 3.0 [1/min], and m_2 = 0.016 [1/min]; for the slow blood curve, a_1 = 3.99 [kg/L], a_2 = 4.78 [kg/L], m_1 = 0.144 [1/min], and m_2 = 0.011 [1/min].

Statistical Analyses

The two-tailed *t* test was used to compare the obtained DCE parameters between different lesion groups. The receiver operating characteristic (ROC) analysis was performed to evaluate the diagnostic capability of heuristic and pharmacokinetic parameters to differentiate between each pair of lesion groups, by using MedCalc (Mariakerke, Belgium). $P < .05$ was considered significant. Pearson correlation was used to correlate K^{trans} and k_{ep} obtained from pharmacokinetic analysis with the heuristic parameters directly measured from the DCE kinetics (maximum enhancement ratio, steepest wash-in ratio, and wash-out slope %).

RESULTS

Lesion Group Comparisons

The wash-out slope was used to determine the DCE kinetic pattern for each case, summarized in Table 1. All 9 myelomas (9 of 9 = 100%) showed the wash-out pattern. Of 22 metastatic cancer, 7 of 22 (32%) showed the wash-out, 11 of 22 (50%) showed the plateau, and 4 of 22 (18%) showed the persistent enhancement pattern. All 7 lymphomas (7 of 7 = 100%) showed the plateau pattern. Of 24 TB cases, only 1 case showed the wash-out (1 of 24 = 4%), 12 of 24 (50%) showed the plateau, and 11 of 24 (46%) showed the persistent enhancement pattern.

The mean ± standard deviation of the analyzed DCE heuristic and pharmacokinetic parameters by using three different blood curves are summarized in Table 2. The mean washout slope was −22% ± 10% for myeloma, 1% ± 0.4% for metastatic cancer, 3% ± 3% for lymphoma, and 7% ± 10% for TB. It can be seen that myeloma has a much higher mean steepest wash-in enhancement ratio compared to the other three groups (1.7 vs 1.0~1.1), and a faster wash-out slope compared to the other three groups (−22% vs 1%~7%). The maximum enhancement ratio was the highest in lymphoma, then myeloma, TB, and the lowest in metastasis.

The pharmacokinetic analysis also showed higher K^{trans} and k_{ep} in the myeloma compared to the other three groups. The differences in the metastatic cancer, lymphoma, and TB groups were not clear, and only the k_{ep} showed a noticeable decreasing trend. The mean k_{ep} [1/min] was 0.88 for myeloma, 0.49 for metastatic cancer, 0.34 for lymphoma, and 0.27 for TB. The distribution of k_{ep} analyzed using the fast blood curve in each lesion group is illustrated in Figure 2.

ROC Diagnostic Comparisons

The diagnostic performance was evaluated using the ROC analysis, done for each pair of lesions. The area under the ROC curve (AUC) with the 95% confidence intervals and the *P* values are listed in Table 3, and the parameter that reaches the significant *P* value is marked. All myelomas showed the wash-out DCE pattern, and as expected, the wash-out slope could be used for distinguishing myeloma from others. The AUC for differentiating myeloma from other lesions was very high, 0.884 with metastatic cancer, and a perfect 1.0 with lymphoma

and TB. The wash-in enhancement ratio was also much higher in myeloma, and the AUC for differentiating myeloma from other lesions was significant as well.

The ROC results for K^{trans} and k_{ep} analyzed using the fast blood curve are also listed in Table 3. Consistent with the clearly noted differences in the DCE kinetic pattern and the wash-out slope, k_{ep} could significantly distinguish myeloma from the other groups, showing AUC = 0.864 with metastatic cancer; a perfect AUC = 1.0 with lymphoma; and 0.995 with TB.

The maximum enhancement is the highest in lymphoma and the lowest in metastasis, and the ROC analysis showed significant differences in myeloma vs metastasis (AUC = 0.81, P = .007) and lymphoma vs metastasis (AUC = 0.91, P = .001).

Correlation of DCE Heuristic Parameters and K^{trans}, k_{ep}

The association between the DCE heuristic and pharmacokinetic parameters was tested with the Pearson correlation. Figure 3 shows the correlation of K^{trans} obtained using the fast blood curve with the maximum enhancement ratio (r = 0.71) and steepest wash-in enhancement ratio (r = 0.85). Figure 4 shows the correlation of k_{ep} obtained using the fast blood curve with the maximum enhancement ratio (r = 0.02) and washout slope (r = 0.92).

DISCUSSION

In this study, we analyzed a retrospective clinical spinal DCEMRI dataset from 62 patients with four diseases (myeloma, metastatic cancer, lymphoma, and TB), so they could be used to evaluate the diagnostic capability of the obtained DCE parameters. For each patient, the heuristic parameters (maximum enhancement, steepest wash-in enhancement, and wash-out slope) and pharmacokinetic parameters (K^{trans} and k_{ep}) were obtained. Because it was difficult to measure the arterial input function for each individual patient, the pharmacokinetic parameters were obtained using three different blood curves (fast, medium, and slow) as references, and the results were compared. In the correlation analysis, k_{ep} was highly correlated with the wash-out slope, and K^{trans} was highly correlated with the wash-in enhancement. It was found that the wash-out slope and k_{ep} analyzed using the fast blood curve had the best group differentiation capability.

The common symptom to these patients was back pain, and MRI was often performed for diagnosis. Osteolytic destruction and soft tissue mass showing heterogeneous enhancements were the most common imaging features shown on pre- and postcontrast enhanced images. Although it was easy to detect the lesion, making a correct diagnosis was difficult. Myeloma and lymphoma might also present as diffuse bone marrow infiltration, but all cases included in this study had clear osteolytic bone destruction and most cases also had soft tissue masses. For spinal TB, the narrowing of intervertebral disk space and paraspinal abscess are typical signs (26,27). However, at an early disease stage when the tuberculous abscess has not yet formed or when the TB has not involved the intervertebral disk, the paraspinal lesion shows as a solid mass and the TB may be misdiagnosed as malignant. Spinal metastasis is the most encountered disease of the spinal lesion, mainly presenting vertebral bone

destruction and soft tissue mass, with rare disc involvement. Similar imaging presentations on conventional MRI make diagnosis of these lesions very challenging (28–31).

Our results showed that DCE-MRI may provide additional information to aid in differential diagnosis. For all cases analyzed in this study, when there was a clear wash-out in the DCE kinetics, the peak enhancement occurred within the first 67 seconds after injection. The total DCE imaging time period in this study varied from 120 to 168 seconds; it was relatively short (<3 minutes), yet sufficient for separating 62 cases into 17 wash-out, 30 plateau, and 15 persistent enhancement patterns. All myeloma cases showed the washout DCE pattern, which was associated with a high vascular volume and a high vascular permeability. Myeloma is a primary bone marrow disease, and it may carry the sinusoidal or discontinuous capillary type that has a very wide endothelial junction, thus a high vascular permeability (32). The washout pattern may also be associated with a high cellular density, which limits the distribution of contrast agents into the extravascular-extracellular space. In histologic examination, spinal myeloma showed high cellular density with little interstitial space. The metastatic cancer was a very heterogeneous group with carcinoma of different origins (10). The 22 metastatic cancer cases showed the wash-out, plateau, and persistent enhancement DCE patterns, suggesting that their histologic presentations varied substantially and showed diverse vascular and cellular properties. All seven lymphoma cases showed the plateau DCE pattern, and among the four groups, it had the highest maximum enhancement indicating a high vascular supply. In 24 cases of TB, only 1 case showed the washout. Inflammatory lesions such as TB have relatively mature vascular structure, less likely to show the wash-out pattern. In pathologic examination, the typical tubercle often showed micro-necrosis, allowing the retention of [Gd] contrast agents, and thus more likely to present the plateau and persistent enhancement DCE patterns. The different vascular and cellular properties revealed by DCE-MRI may help the diagnosis and staging of vertebral lesions (8–16).

In the literature, quite a few studies have applied DCEMRI to characterize various spinal lesions for diagnosis, disease staging, therapy monitoring, and prediction of prognosis (8–20). The diagnostic features may provide helpful information for evaluating the extent of the disease for surgical and other adjuvant treatment planning. Also, several studies have applied DCE-MRI to monitor treatment-induced changes using different therapies, for example, chemotherapy (17), radiation therapy (20), angiogenic therapy (19), and stem cell transplantation (16). DCE-MRI parameters have been shown to be associated with prognosis and survival of patients, which might be related to the angiogenesis of the disease (14–18,33). It was found that a higher microvessel density was correlated with higher tumor grade, worse prognosis, and shorter survival in myeloma patients (34–36). In addition to providing important diagnostic or prognostic information, DCEMRI could also evaluate focal vs diffuse patterns (37) and was recommended as a supplement for the clinical staging of myeloma (38).

There were two main analysis methods for DCE-MRI: heuristic and pharmacokinetic, similar to what we presented in this study. Regardless of the analysis methods, most studies found DCE parameters showing significant differences between diseased and normal bone marrow, or between different lesions(8–15).Khadem et al. used heuristic DCE analysis to

discriminate hypervascular from hypovascular spinal metastases (12), and later Saha et al. from the same research group showed that pharmacokinetic parameters analyzed by using a commercial software (NordicNeuroLab) could distinguish hypervascular renal cell carcinoma from hypovascular prostate carcinoma (13). DCEMRI using heuristic analysis and model fitting has been applied to characterize vascular properties of different hematologic malignancies (eg, myeloma and lymphoma) with different grades of bone marrow involvement (8,9,15). We have shown that DCE parameters of metastatic cancers were significantly different from those of myeloma (10) and inflammatory TB (11). Unfortunately, there were few studies in the literature that reported the diagnosis of spinal masses using DCE-MRI for comparison with our findings.

For pharmacokinetic analysis, several software such as Syngo Tissue 4D, provides the fitting function to obtain K^{trans} and k_{ep}. The operator can choose a vessel ROI to measure the arterial input function of each individual patient, or use a predefined population-based blood curve function as the reference (21–23). Our results showed that the fitted parameters K^{trans} and k_{ep} using different blood curves have different values. With the short DCE time period of 3 minutes for the spinal lesions, the analysis done by using the fast blood curve was more suitable compared to the medium or the slow blood curve. In our study we have shown that K^{trans} was highly correlated with the wash-in enhancement, and k_{ep} was highly correlated with the wash-out slope; therefore, performing the sophisticated pharmacokinetic analysis was not necessary. The heuristic parameters that could be easily measured from the DCE enhancement time course could provide very helpful diagnostic information. Among all analyzed parameters, a simple wash-out slope calculated by using the intensity at the last DCE time point and the intensity at 1 minute after the contrast injection has a very high diagnostic accuracy. This can be easily calculated in a clinical setting as a diagnostic marker.

There were several limitations in this study. This was a retrospective study using patients identified from our clinical MRI database, with small number of myeloma and lymphoma patients. Although they were common diseases, it was rare to present as spinal lesions that caused pain without other symptoms to be referred to for diagnosis by MRI; therefore, we did not have many spinal myeloma and lymphoma cases. We only presented DCE-MRI results in this study, not analyzing the morphologic features—mainly because they could not be quantified. There were substantial overlaps in the analyzed DCE parameters between different lesion groups, but we have clearly shown that DCE-MRI can provide very helpful information to characterize detected lesions to aid in diagnosis.

CONCLUSIONS

We have shown that DCE-MRI may help in differentiating spinal lesions that show similar features on pre- and postcontrast MRI. All myeloma showed the wash-out and all lymphoma showed the plateau patterns; metastatic cancers were heterogeneous; and the inflammatory TB was most likely to show the persistent enhancement pattern. The pharmacokinetic analysis using the standard blood curves as references could extract quantitative parameters that were correlated with wash-in and wash-out features in the DCE kinetics. Of all analyzed parameters, the wash-out slope and k_{ep} had the best differential diagnostic capability in ROC analysis. Because the pharmacokinetic parameters were highly correlated with heuristic

parameters, it may not be necessary to perform the much more sophisticated DCE-MRI pharmacokinetic fitting for diagnosis. It is difficult to diagnose lesions in the spine, and DCE-MRI may provide very helpful information for guiding biopsy and planning of surgery and subsequent adjuvant treatments.

ACKNOWLEDGMENTS

Funding Support: This work was supported in part by the NIH/NCI R01 CA127927, P30 CA62203, the National Natural Science Foundation of China (81471634), and the Beijing Natural Science Foundation (7164309).

REFERENCES

1. Turnbull LW. Dynamic contrast-enhanced MRI in the diagnosis and management of breast cancer. NMR Biomed 2009; 22:28–39. [PubMed: 18654999]
2. Verma S, Turkbey B, Muradyan N, et al. Overview of dynamic contrast-enhanced MRI in prostate cancer diagnosis and management. AJR Am J Roentgenol 2012; 198:1277–1288. [PubMed: 22623539]
3. Su MY, Chen JH. Quantitative measurements of tracer transport parameters using dynamic contrast-enhanced MRI as vascular perfusion and permeability indices in cancer imaging, Chapter10 In: Tugan Muftuler L, ed. Quantifying morphology and physiology of the human body using MRI. Boca Raton, FL: Taylor & Francis, 2013.
4. Khalifa F, Soliman A, El-Baz A, et al. Models and methods for analyzing DCE-MRI: a review. Med Phys 2014; 41:124301. [PubMed: 25471985]
5. Tofts PS, Kermode AG. Measurement of the blood-brain barrier permeability and leakage space using dynamic MR imaging. 1. Fundamental concepts. Magn Reson Med 1991; 17:357–367. [PubMed: 2062210]
6. Tofts PS. Modeling tracer kinetics in dynamic Gd-DTPA MR imaging. J Magn Reson Imaging 1997; 7:91–101. [PubMed: 9039598]
7. Taylor JS, Tofts PS, Port R, et al. MR imaging of tumor microcirculation: promise for the new millennium. J Magn Reson Imaging 1999; 10:903–907. [PubMed: 10581502]
8. Moulopoulos LA, Maris TG, Papanikolaou N, et al. Detection of malignant bone marrow involvement with dynamic contrast-enhanced magnetic resonance imaging. Ann Oncol 2003; 14:152–158. [PubMed: 12488307]
9. Rahmouni A, Montazel JL, Divine M, et al. Bone marrow with diffuse tumor infiltration in patients with lymphoproliferative diseases: dynamic gadolinium-enhanced MR imaging. Radiology 2003; 229:710–717. [PubMed: 14593191]
10. Lang N, Su MY, Yu HJ, et al. Differentiation of myeloma and metastatic cancer in the spine using dynamic contrast-enhanced MRI. Magn Reson Imaging 2013; 31:1285–1291. [PubMed: 23290477]
11. Lang N, Su MY, Yu HJ, et al. Differentiation of tuberculosis and metastatic cancer in the spine using dynamic contrast-enhanced MRI. Eur Spine J 2015; 24:1729–1737. [PubMed: 25749725]
12. Khadem NR, Karimi S, Peck KK, et al. Characterizing hypervascular and hypovascular metastases and normal bone marrow of the spine using dynamic contrast-enhanced MR imaging. AJNR Am J Neuroradiol 2012; 33:2178–2185. [PubMed: 22555585]
13. Saha A, Peck KK, Lis E, et al. Magnetic resonance perfusion characteristics of hypervascular renal and hypovascular prostate spinal metastases: clinical utilities and implications. Spine 2014; 39:E1433–E1440. [PubMed: 25188594]
14. Stäbler A, Baur A, Bartl R, et al. Contrast enhancement and quantitative signal analysis in MR imaging of multiple myeloma: assessment of focal and diffuse growth patterns in marrow correlated with biopsies and survival rates. AJR Am J Roentgenol 1996; 167: 1029–1036. [PubMed: 8819407]

15. Zha Y, Li M, Yang J. Dynamic contrast enhanced magnetic resonance imaging of diffuse spinal bone marrow infiltration in patients with hematological malignancies. Korean J Radiol 2010; 11:187–194. [PubMed: 20191066]
16. Dutoit JC, Vanderkerken MA, Verstraete KL. Value of whole body MRI and dynamic contrast enhanced MRI in the diagnosis, follow-up and evaluation of disease activity and extent in multiple myeloma. Eur J Radiol 2013; 82:1444–1452. [PubMed: 23726124]
17. Hillengass J, Wasser K, Delorme S, et al. Lumbar bone marrow microcirculation measurements from dynamic contrast-enhanced magnetic resonance imaging is a predictor of event-free survival in progressive multiple myeloma. Clin Cancer Res 2007; 13(2 Pt 1):475–481. [PubMed: 17255268]
18. Chen BB, Hsu CY, Yu CW, et al. Dynamic contrast-enhanced MR imaging measurement of vertebral bone marrow perfusion may be indicator of outcome of acute myeloid leukemia patients in remission. Radiology 2011; 258:821–831. [PubMed: 21212370]
19. Zechmann CM, Traine L, Meissner T, et al. Parametric histogram analysis of dynamic contrast-enhanced MRI in multiple myeloma: a technique to evaluate angiogenic response to therapy? Acad Radiol 2012; 19: 100–108. [PubMed: 22142682]
20. Chu S, Karimi S, Peck KK, et al. Measurement of blood perfusion in spinal metastases with dynamic contrast-enhanced magnetic resonance imaging: evaluation of tumor response to radiation therapy. Spine 2013; 38: E1418–E1424. [PubMed: 23873238]
21. Parker GJ, Roberts C, Macdonald A, et al. Experimentally-derived functional form for a population-averaged high-temporal-resolution arterial input function for dynamic contrast-enhanced MRI. Magn Reson Med 2006; 56:993–1000. [PubMed: 17036301]
22. Orton MR, d'Arcy JA, Walker-Samuel S, et al. Computationally efficient vascular input function models for quantitative kinetic modelling using DCE-MRI. Phys Med Biol 2008; 53:1225–1239. [PubMed: 18296759]
23. Weinmann HJ, Laniado M, Mützel W. Pharmacokinetics of GdDTPA/dimeglumine after intravenous injection into healthy volunteers. Physiol Chem Phys Med NMR 1984; 16:167–172. [PubMed: 6505043]
24. Cheng HL. Investigation and optimization of parameter accuracy in dynamic contrast-enhanced MRI. J Magn Reson Imaging 2008; 28: 736–743. [PubMed: 18777534]
25. Ashton E, Raunig D, Ng C, et al. Scan-rescan variability in perfusion assessment of tumors in MRI using both model and data-derived arterial input functions. J Magn Reson Imaging 2008; 28:791–796. [PubMed: 18777526]
26. Zheng CY, Liu DX, Luo SW, et al. Imaging presentation highly manifested as tuberculosis in a case of spinal metastatic carcinoma. Orthopedics 2011; 34:e436–e438. [PubMed: 21815592]
27. Yu Y, Wang X, Du B, et al. Isolated atypical spinal tuberculosis mistaken for neoplasia: case report and literature review. Eur Spine J 2013; 22 Suppl 3:S302–S305. [PubMed: 22531896]
28. Erlemann R, Reiser MF, Peters PE, et al. Musculoskeletal neoplasms: static and dynamic Gd-DTPA-enhanced MR imaging. Radiology 1989; 171:767–773. [PubMed: 2717749]
29. Lang P, Honda G, Roberts T, et al. Musculoskeletal neoplasm: perineoplastic edema versus tumor on dynamic postcontrast MR images with spatial mapping of instantaneous enhancement rates. Radiology 1995; 197:831–839. [PubMed: 7480764]
30. May DA, Good RB, Smith DK, et al. MR imaging of musculoskeletal tumors and tumor mimickers with intravenous gadolinium: experience with 242 patients. Skeletal Radiol 1997; 26:2–15. [PubMed: 9040136]
31. Geirnaerdt MJ, Hogendoorn PC, Bloem JL, et al. Cartilaginous tumors: fast contrast-enhanced MR imaging. Radiology 2000; 214:539–546. [PubMed: 10671608]
32. Sarin H Physiologic upper limits of pore size of different blood capillary types and another perspective on the dual pore theory of microvascular permeability. J Angiogenes Res 2010; 2:14. [PubMed: 20701757]
33. Moehler TM, Neben K, Ho AD, et al. Angiogenesis in hematologic malignancies. Ann Hematol 2001; 80:695–705. [PubMed: 11797109]
34. Rajkumar SV, Leong T, Roche PC, et al. Prognostic value of bone marrow angiogenesis in multiple myeloma. Clin Cancer Res 2000; 6:3111–3116. [PubMed: 10955791]

35. Munshi NC, Wilson C. Increased bone marrow microvessel density in newly diagnosed multiple myeloma carries a poor prognosis. Semin Oncol 2001; 28:565–569. [PubMed: 11740810]

36. Kimlinger T, Kline M, Kumar S, et al. Differential expression of vascular endothelial growth factors and their receptors in multiple myeloma. Haematologica 2006; 91:1033–1040. [PubMed: 16870555]

37. Moehler TM, Hawighorst H, Neben K, et al. Bone marrow microcirculation analysis in multiple myeloma by contrast-enhanced dynamic magnetic resonance imaging. Int J Cancer 2001; 93:862–868. [PubMed: 11519049]

38. Baur A, Stäbler A, Nagel D, et al. Magnetic resonance imaging as a supplement for the clinical staging system of Durie and Salmon? Cancer 2002; 95:1334–1345. [PubMed: 12216103]

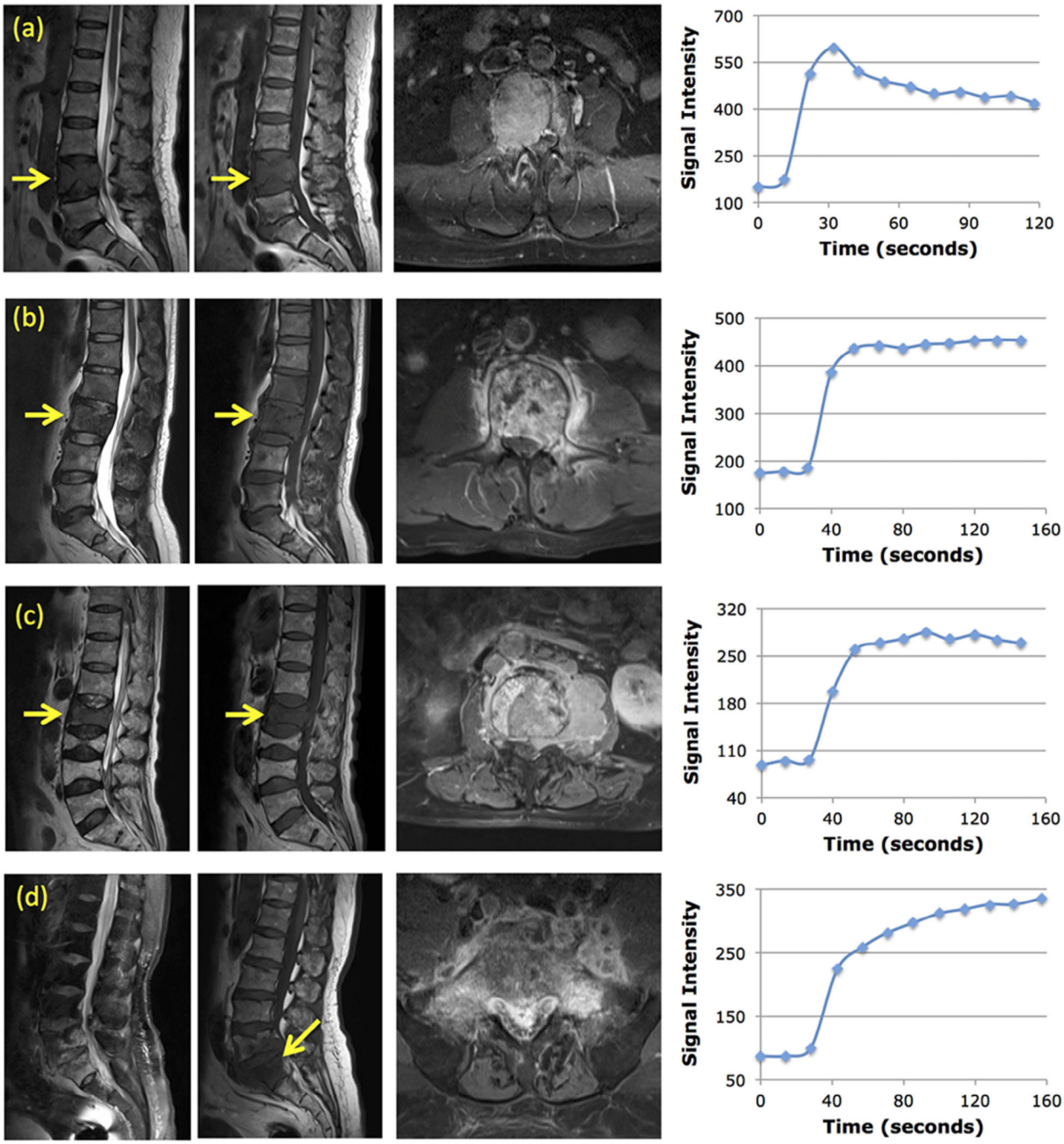

Figure 1.

Four case examples. For each case, from left to right, the sagittal T2-weighted, T1-weighted, axial contrast-enhanced images, and the signal intensity time course measured from a region of interest placed on the strongest enhancement area. **(a)** A 56-year-old woman with myeloma. The DCE kinetics shows the wash-out pattern, with K^{trans} = 0.155/min, k_{ep} = 1.10/min. **(b)** A 45-year-old man with metastatic lung cancer. The DCE kinetics shows the plateau pattern, with K^{trans} = 0.070/min, k_{ep} = 0.37/min. **(c)** A 71-year-old man with lymphoma. The DCE kinetics shows the plateau pattern, with K^{trans} = 0.093/min, k_{ep} = 0.39/

min. **(d)** A 67-year-old man with tuberculosis. The DCE kinetics shows the persistent enhancement pattern, with K^{trans} = 0.086/min, k_{ep} = 0.10/min.

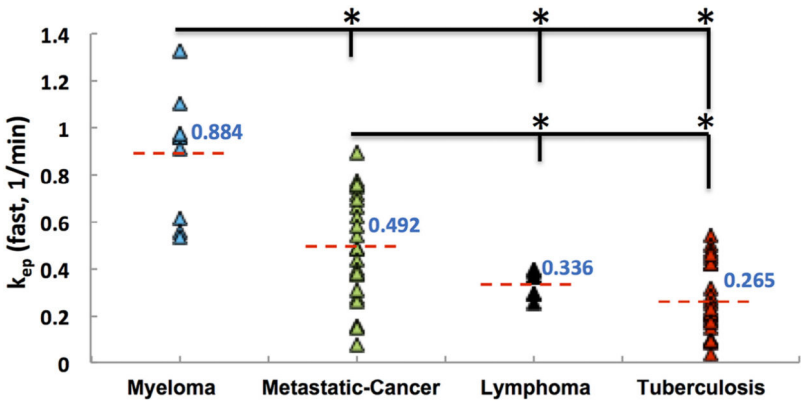

Figure 2.

The distribution of k_{ep} analyzed using the fast blood curve in the four lesion groups. The mean k_{ep} is the highest in the myeloma group and the lowest in the tuberculosis group. Except for lymphoma vs TB, all other pairwise comparisons are significant, marked with *.

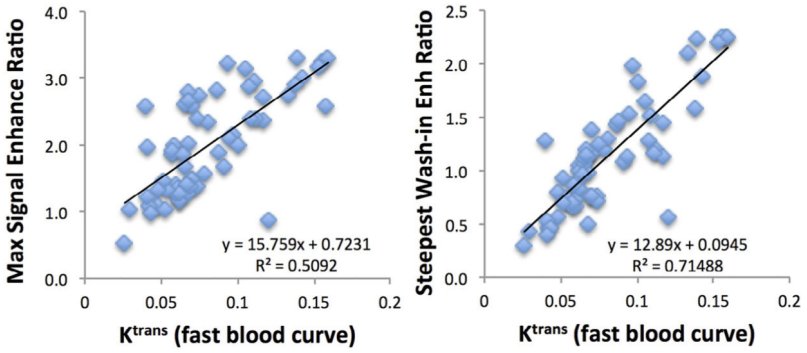

Figure 3.

The correlation of K^{trans} obtained using the fast blood curve with the maximum enhancement ratio and the steepest wash-in enhancement ratio. K^{trans} is strongly correlated with steepest washin enhancement with r = 0.85 (R^2 = 0.71) and also with maximum enhancement with a lower r = 0.71 (R^2 = 0.51).

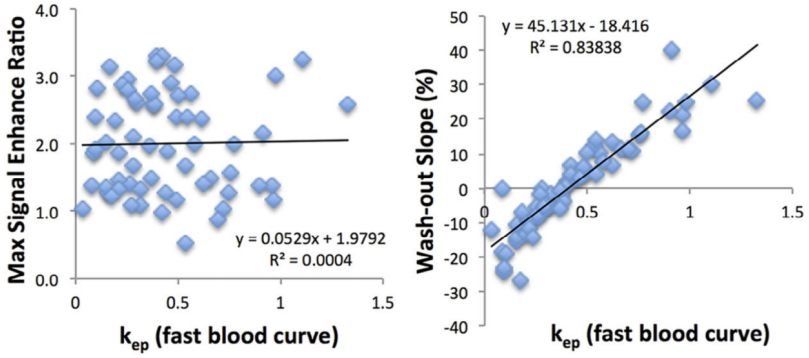

Figure 4.

The correlation of k_{ep} obtained using the fast blood curve with the maximum enhancement ratio and the washout slope (%). It can be seen that k_{ep} is not associated with the maximum enhancement at all with r = 0.02 (R^2 = 0.0004), and it has a high correlation with the washout slope with r = 0.92 (R^2 = 0.84).

Table 1.

The Distribution of Enhancement Kinetic Patterns in the Four Lesion Groups

	Wash-out *n* (%)	**Plateau *n* (%)**	**Persistent *n* (%)**
Myeloma (*n* = 9)	9 (100)	0	0
Metastasis (*n* = 22)	7 (32)	11 (50)	4 (18)
Lymphoma (*n* = 7)	0	7 (100)	0
Tuberculosis (*n* = 24)	1 (4)	12 (50)	11 (46)

Table 2.

Heuristic Parameters Analyzed From DCE Enhancement Kinetics of Lesions in Four Disease Groups, and the Pharmacokinetic Parameters Obtained by Using the Fast, Medium, and Slow Blood Curves (Mean ± Standard Deviation Is Shown)

	Maximum Enhancement Ratio	Wash-in Enhancement Ratio	Wash-out Slope	K^{trans}-Fast (1/min)	K^{trans}-Medium (1/min)	K^{trans}-Slow (1/min)	k_{ep}-Fast (1/min)	k_{ep}-Medium (1/min)	k_{ep}-Slow (1/min)
Myeloma (n= 9)	2.3 ± 0.7	1.7 ± 0.5	−22±10%	0.114 ± 0.036	0.29 ± 0.15	1.24 ± 0.77	0.88 ± 0.26	1.86 ± 0.88	6.50 ± 3.13
Metastasis (n = 22)	1.7 ± 0.6	1.1 ± 0.4	1 ± 0.4%	0.077 ± 0.028	0.18 ± 0.07	0.66 ± 0.32	0.49 ± 0.23	1.09 ± 0.39	4.22 ± 1.46
Lymphoma (n = 7)	2.7 ± 0.4	1.0 ± 0.3	3 ± 3%	0.068 ± 0.016	0.16 ± 0.03	0.67 ± 0.17	0.34 ± 0.06	0.83 ± 0.07	4.27 ± 0.79
Tuberculosis (n = 24)	2.0 ± 0.8	1.0 ± 0.6	7 ± 10%	0.077 ± 0.036	0.17 ± 0.08	0.77 ± 0.63	0.27 ± 0.15	0.72 ± 0.25	3.90 ± 2.23

DCE, dynamic contrast-enhanced.

Table 3.

The Area Under the ROC Curve (AUC) to Differentiate Between Different Disease Groups Using Heuristic and Pharmacokinetic Parameters Measured From DCE Kinetics

	Maximum Enhancement Ratio		Wash-in Enhancement Ratio		Wash-out Slope		K^{trans}-Fast (1/min)		k_{ep}-Fast(1/min)	
	AUC (95% CI)	***P* Value**	**AUC (95% CI)**	***P* Value**	**AUC (95% CI)**	***P* Value**	**AUC (95% CI)**	***P* Value**	**AUC (95% CI)**	***P* Value**
Myeloma vs. metastasis	0.810 *(0.658-.963)	.007	0.803 *(0.638–0.968)	.009	0.884 *(0.766–1.00)	.001	0.798 *(0.632–0.964)	.010	0.864 *(0.717–1.00)	.002
Myeloma vs lymphoma	0.683 (0.408–0.957)	.223	0.810 *(0.588–1.00)	.039	1.000 *(1.00–1.00)	.001	0.841 *(0.636–1.00)	.023	1.000 *(1.00–1.00)	.001
Myeloma vs tuberculosis (TB)	0.583 (0.373–0.793)	.467	0.737 *(0.533–0.942)	.041	1.000 *(1.00–1.00)	.001	0.782 *(0.617–0.948)	.014	0.995 *(0.980–1.00)	.001
Metastasis vs lymphoma	0.909 *(0.793–1.00)	.001	0.435 (0.200–0.671)	.610	0.734 (0.558–0.910)	.067	0.487 (0.263–0.711)	.919	0.734 (0.558–0.910)	.067
Metastasis vs TB	0.631 (0.466–0.796)	.129	0.602 (0.433–0.771)	.235	0.741 *(0.595–0.886)	.005	0.464 (0.293–0.636)	.676	0.780 *(0.643–0.918)	.001
Lymphoma vs TB	0.702 (0.521–0.884)	.108	0.521 (0.299–0.742)	.869	0.607 (0.419–0.796)	.395	0.512 (0.300–0.724)	.925	0.673 (0.490–0.855)	.171

95% CI: 95% confidence intervals shown in brackets.

*Reaching the significant level at $P<.05$.